

# Structure and Function of the Conserved 690 Hairpin in *Escherichia coli* 16 S Ribosomal RNA. III.† Functional Analysis of the 690 Loop

Svetlana V. Morosyuk<sup>1</sup>, John SantaLucia Jr<sup>1</sup> and Philip R. Cunningham<sup>2\*</sup>

<sup>1</sup>Department of Chemistry  
Wayne State University  
Detroit, MI, 48202, USA

<sup>2</sup>Department of Biological  
Sciences, Wayne State  
University, Detroit, MI  
48202, USA

An instant-evolution experiment was performed on the eight nucleotides comprising the loop region of the 690 hairpin in *Escherichia coli* 16 S ribosomal RNA. Positions 690 to 697 were randomly mutated and 101 unique functional mutants were isolated, sequenced and analyzed for function *in vivo*. Non-random nucleotide distributions were observed at each of the mutated positions except 693 and 694. Nucleotide identity significantly affected ribosome function at positions 690, 695, 696 and 697. Pyrimidines were absent at position 696 in the instant-evolution pool as were C at position 691 and G at position 697. A highly significant covariation was observed between nucleotides 690 and 697. No functional double mutants at positions 691 and 696 were obtained from the instant-evolution pool. In our NMR structure of the 690 loop, both the G690·U697 and G691·A696 form sheared hydrogen-bonded mismatches. To further examine the functional constraints between these paired nucleotides, one set of site-directed mutations was constructed at positions 690:697 and another set was constructed at positions 691:696. Functional analysis of the site-directed mutants is consistent with our instant-evolution findings and revealed constraints on the placement of specific functional groups observed in the NMR structure. Ten instant-evolution mutants were isolated that are more functional than the wild-type. Hyperactivity in these mutants correlates with a single mutation at position 693.

© 2001 Academic Press

\*Corresponding author

Keywords: ribosomal RNA; 690 loop; instant evolution; mutation; function

## Introduction

Comparative sequence analysis is a powerful tool for RNA secondary structure prediction. This approach has been used effectively to determine the secondary structures of several large RNAs including the ribosomal RNAs (Gutell *et al.*, 1994), group I introns (Michel & Westhof, 1990), ribonuclease P RNA (Brown *et al.*, 1996), and tRNAs (Sprinzl *et al.*, 1996). Phylogenetic identification of helical regions was initially based upon covariations involving canonical Watson-Crick base-pairs. Improvements in computational methods for comparative

sequence analysis and expansion of sequence databases have allowed extension of secondary structure prediction to include non-canonical base-pairs and base-triplets (Conn *et al.*, 1998; Gautheret *et al.*, 1995; Gutell & Woese, 1990; Haselman *et al.*, 1989; Larsen, 1992). Covariation analysis of functionally important regions of RNAs, however, is limited because these sequences are often highly conserved or invariant. In addition, base to base covariations are context-dependent. The effect of context is particularly significant for non-canonical or mismatch pairs, where nucleotides participate in stacking and H-bonding interactions with more than one nucleotide. Thus, a single nucleotide substitution may dramatically alter RNA tertiary structure. For such sequences, maintaining tertiary structure and molecular function requires multiple, simultaneous substitutions of the interacting nucleotides, an event that is unlikely to occur through spontaneous mutations *in vivo*.

†Paper II in this series is the accompanying paper, Morosyuk *et al.* (2001).

Abbreviations used: CAT, chloramphenicol acetyl transferase; GFP, green fluorescent protein.

E-mail address of the corresponding author: [phil@biology.biosci.wayne.edu](mailto:phil@biology.biosci.wayne.edu)

To identify functionally important nucleotides and structural motifs, we developed an *in vivo* method to isolate and analyze functional sequence variants of 16 S ribosomal RNA, termed instant evolution (Lee *et al.*, 1996, 1997). In an instant-evolution experiment all of the nucleotide positions in a conserved region of RNA are simultaneously randomly mutated and the functional sequences are isolated and analyzed. This permits the isolation of functional sequences that show more variability than those found in nature. In this way, instant evolution allows for the identification of important structural motifs even when they are located within highly conserved functional sequences. The minimum level of function among the instant-evolution pool is determined by the selection procedure. By selecting mutants with a wide range of activities, the effects of substitutions at each position may be correlated with ribosome function. The instant-evolution approach was previously used to determine the key functional and structural elements of the 790 loop (Lee *et al.*, 1997) and base-pairing interactions in the 690 region in 16 S rRNA (Morosyuk *et al.*, 2000).

Here, we investigated the conserved loop of helix 23b of 16 S rRNA. The 690 loop terminates helix 23b in the central domain of *Escherichia coli* 16 S rRNA (Figure 1) and has been implicated in tRNA binding at the P-site (Doring *et al.*, 1994; Joseph *et al.*, 1997; Moazed & Noller, 1986, 1990; Osswald *et al.*, 1995; Rinke-Appel *et al.*, 1995), subunit association (Cate *et al.*, 1999; Merryman *et al.*, 1999), interactions with the 790 loop (Atmadja *et al.*, 1986; Clemons *et al.*, 1999), IF3 binding (Muralikrishna & Wickstrom, 1989; Pon *et al.*, 1982; Stoffler-Meilicke & Stoffler, 1987) and interactions with S11 protein (Agalarov & Williamson, 2000; Mueller &

Brimacombe, 1997; Powers & Noller, 1995; Stern *et al.*, 1988). The 690 loop nucleotides were also shown to affect binding of the antibiotics pactamycin and edeine, which inhibit initiation of protein synthesis (Egebjerg & Garrett, 1991; Mankin, 1997; Oehler *et al.*, 1997; Woodcock *et al.*, 1991). Instant evolution was used to identify functional sequence variants of the 690 loop and to determine the sequence and structural elements required for ribosome function. Comparison of the instant-evolution data presented here with the NMR solution structure presented in the accompanying paper (Morosyuk *et al.*, 2001) and the recently determined X-ray crystal structures of the small subunit (Schluenzen *et al.*, 2000; Wimberly *et al.*, 2000) allows correlation of specific sequence elements in the 690 loop with ribosome function.

## Results

### Random mutagenesis and selection of functional mutants

To examine the role of the 690 loop in protein synthesis, an instant-evolution experiment was performed in which nucleotides 690 to 697 of *E. coli* 16 S RNA were randomly mutated and functional sequence combinations were selected and analyzed *in vivo*. The nucleotides were mutated using PCR and the PCR products were cloned into a derivative of the expression vector pRNA122 (Lee *et al.*, 1996, 1997). In this vector, pRNA123, the chloramphenicol acetyltransferase (CAT) mRNA and the green fluorescent protein (GFP) mRNA (Chalfie *et al.*, 1994) are translated only by plasmid-derived ribosomes. The CAT protein renders cells resistant to chloramphenicol and is used to select functional

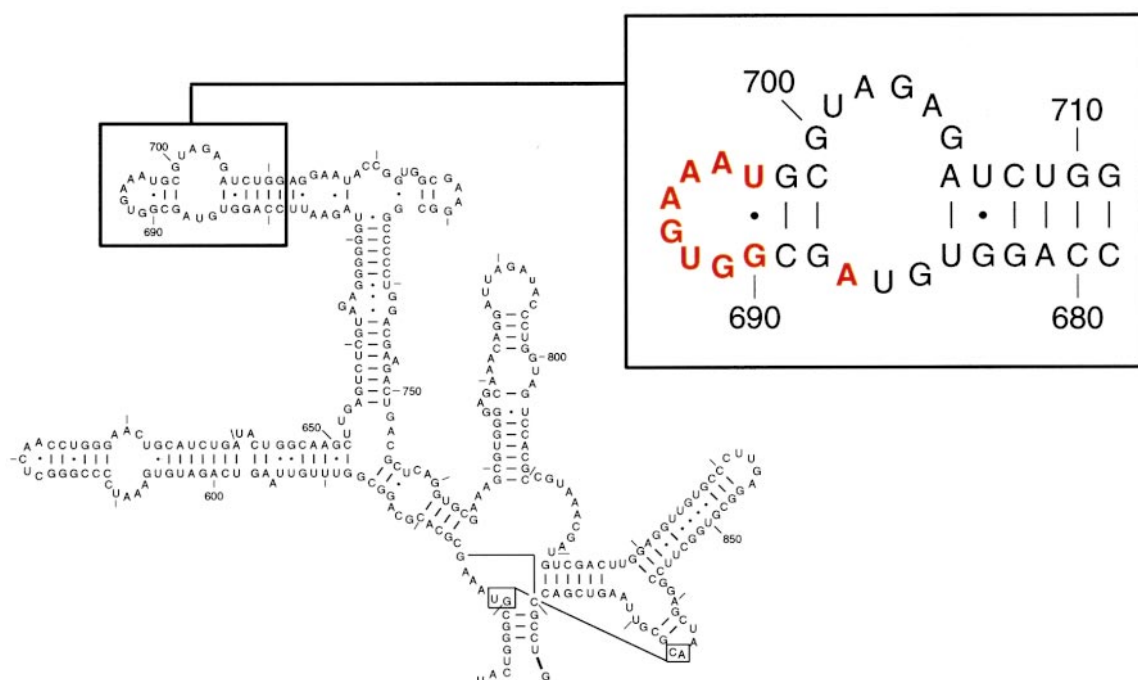


**Figure 1.** The central domain of *E. coli* 16 S ribosomal RNA showing the 690 region (boxed). Nucleotides in red are conserved in >95% of all bacteria (Van de Peer *et al.*, 1999).

mutants. GFP allows rapid and accurate determination of ribosome function by directly measuring fluorescence in whole cells. Equal distribution of the four nucleotides at each randomized position in the mutant pool was confirmed by sequence analysis of a sample of the plasmid library prior to selection (Figure 2(b)).

To determine the optimal chloramphenicol concentration for selection, 8000-20,000 transformants were plated on selection medium containing 0, 50, 100, 150, 200 or 300  $\mu\text{g}/\text{ml}$  chloramphenicol. Following incubation, the survivors were counted and assayed for GFP translation (not shown). From these data, 200  $\mu\text{g}/\text{ml}$  chloramphenicol was determined as the optimal concentration for selection of the 690 loop instant-evolution mutants (see Materials and Methods). Mutants were selected, sequenced, and assayed for ribosome function by measuring the amount of GFP produced by each mutant strain. A total of 500,000 transformants were obtained to ensure that all of the mutant sequences were represented in the original pool with >99.9% confidence (Clarke & Carbon, 1976). Out of these 500,000 transformants, only 186 clones containing 101 unique sequences survived the selection (Table 1). The number of mutations per survivor ranged from one to six (Table 1) and 72 of the isolates had three or four mutations (Figure 3(a)). The level of function ranged from 22 to 124% of the wild-type (Table 1). Overall, the number of mutations in the 690 loop was inversely proportional to the level of ribosome function (Figure 3(b)). It is interesting that seven mutants were as functional as wild-type, and ten of the mutants produced more GFP than the wild-type. Although most of these hyperactive mutants contained multiple mutations, all of them contained nucleotide substitutions at position 693 and one of them (Table 1, sequence 2) contained a single G693U substitution and produced 22% more GFP than the wild-type. These data suggest that mutations at position 693 affect the rate of protein synthesis (see Discussion).

### Nucleotide distribution

A comparison of the instant-evolution sequence data with the phylogenetic data is shown in Table 2. The instant-evolution sequences showed significantly more variability than those found in nature. This is presumably because all of the positions in the loop were mutated simultaneously and because the mutants were selected at a chloramphenicol concentration that allowed suboptimal sequences to be isolated (Lee *et al.*, 1997).

The instant-evolution survivors showed non-random nucleotide distributions at each mutated position, except 693 and 694 (Table 2 and Figure 4(a)). For comparison, a subset of the 101 instant-evolution mutants containing 51 mutants with protein synthesis activities  $\geq 65\%$  of the wild-type were also analyzed (Table 2, parentheses). Nucleotide distribution among the 51 highly functional mutants was similar to that observed in the entire instant-evolution pool of 101 mutants. No mutants containing a C at position 690 were present in the highly functional subset of instant-evolution mutants. Statistical analysis of nucleotide variation at each of the other positions, however, was consistent with the decrease in sample size. None of the functional mutants isolated has a C at position 691, U or C at position 696, or G at position 697. Each of these substitutions would disrupt interactions of the 690 loop with nucleotides in the 790 stem loop of 16 S RNA and with ribosomal protein S11 observed in recently published crystal structures of the small ribosomal subunit (Schluenzen *et al.*, 2000; Wimberly *et al.*, 2000) (see Discussion). The mean activities of all mutants at each position were compared by single-factor analysis of variance (ANOVA) (Table 3) to determine if nucleotide identity at a given position affected ribosome function (Lee *et al.*, 1997). Positions where nucleotide substitutions significantly affect ribosome function among the instant-evolution mutants are 690, 695, 696, and 697 (Table 3 and Figure 4(a), boxed nucleotides). Since some nucleotides were

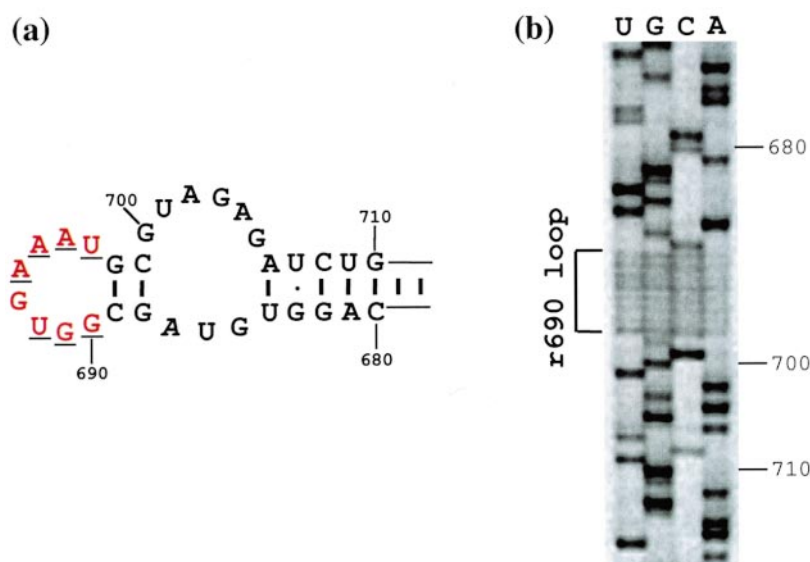


**Figure 2.** Mutation of the 690 loop nucleotides. (a) The 690 region showing mutated nucleotides (red). Sequence conservation >95% is indicated by underlining. (b) Sequencing gel showing equal distribution of the nucleotides at the eight mutated positions of the 690 loop prior to selection.

**Table 1.** Sequence and function of the functional 690 loop mutants

Sequence number	Nucleotide sequence <sup>a</sup>									Number of mutations <sup>b</sup>	Percentage function <sup>c</sup>
	690	691	692	693	694	695	696	697			
WT <sup>d</sup>	G	G	U	G	A	A	A	U	0	100	
1	G	G	U	A	U	A	A	U	2	124.0(±4.8)	
2	G	G	U	U	A	A	A	U	1	122.2(±1.4)	
3	G	G	U	A	C	A	A	U	2	121.4(±2.2)	
4	G	G	U	U	C	A	A	U	2	112.8(±1.9)	
5	G	G	U	U	U	C	A	U	3	112.4(±4.1)	
6	G	G	U	U	A	A	A	U	2	112.1(±4.3)	
7	G	G	U	C	U	A	A	U	2	111.1(±4.8)	
8	G	G	U	A	C	U	A	U	3	108.0(±1.2)	
9	G	G	U	U	U	C	A	U	3	106.6(±3.7)	
10	G	G	U	A	C	U	A	U	3	106.1(±3.9)	
11	G	G	U	C	C	U	A	U	3	102.2(±5.4)	
12	G	G	C	U	C	A	A	U	3	100.9(±2.0)	
13	G	G	U	U	C	A	A	U	3	100.9(±4.7)	
14	G	G	U	G	U	A	A	U	2	100.6(±4.2)	
15	G	G	U	G	C	U	A	U	2	100.5(±4.5)	
16	G	U	U	C	A	A	A	U	2	99.2(±0.2)	
17	G	A	U	C	A	A	A	U	1	98.3(±4.4)	
18	A	C	U	C	A	A	A	A	4	94.6(±1.4)	
19	A	G	C	A	G	C	A	U	4	93.5(±1.4)	
20	G	G	U	C	C	C	A	U	3	92.9(±3.2)	
21	G	G	A	C	A	A	A	U	4	90.2(±2.4)	
22	G	G	A	C	G	C	A	U	2	89.1(±4.0)	
23	G	U	U	C	A	A	A	U	3	88.3(±4.2)	
24	G	U	U	C	C	C	A	U	3	87.9(±1.7)	
25	G	U	U	C	C	A	A	U	2	86.2(±1.6)	
26	G	U	U	C	G	U	A	U	3	85.3(±0.4)	
27	G	G	U	C	A	U	A	U	1	85.1(±2.0)	
28	A	G	U	C	G	A	A	U	3	84.5(±3.3)	
29	G	A	U	U	A	A	A	U	3	83.9(±4.6)	
30	A	G	C	U	A	U	A	U	3	81.3(±4.3)	
31	A	G	U	C	A	U	A	U	3	77.7(±3.2)	
32	A	G	U	U	U	U	A	U	3	75.7(±0.9)	
33	G	G	U	C	G	U	G	U	3	75.6(±2.4)	
34	G	G	U	C	C	U	G	U	4	74.4(±1.6)	
35	A	G	U	U	U	A	A	A	4	71.5(±0.1)	
36	A	G	U	U	U	A	A	U	3	71.1(±2.9)	
37	U	G	U	A	U	A	A	C	4	71.1(±0.7)	
38	U	G	U	A	A	A	A	U	3	70.6(±2.6)	
39	A	G	A	C	G	C	A	U	4	70.0(±0.2)	
40	G	G	C	C	A	A	A	U	3	69.6(±2.8)	
41	A	G	U	A	A	A	A	A	4	69.0(±2.9)	
42	A	G	U	U	G	C	A	U	4	68.8(±1.9)	
43	G	G	U	U	U	C	G	U	4	68.5(±2.0)	
44	G	U	U	U	G	U	A	U	4	68.2(±1.5)	
45	U	G	U	G	A	A	A	C	2	67.5(±1.0)	
46	U	G	U	G	A	U	A	C	4	67.5(±2.0)	
47	G	G	U	A	U	A	G	U	3	67.2(±2.8)	
48	G	G	U	C	C	A	G	U	3	66.1(±4.3)	
49	A	A	U	A	G	A	A	U	4	65.7(±2.7)	
50	A	C	U	A	G	C	A	C	3	65.6(±4.4)	
51	A	A	U	U	U	C	A	U	3	65.5(±2.7)	
52	G	C	U	G	C	A	G	U	2	64.2(±3.4)	
53	G	G	G	C	U	A	A	U	3	64.1(±0.6)	
54	U	G	U	C	C	A	A	C	4	63.9(±0.1)	
55	G	G	C	C	U	U	A	U	3	63.5(±3.1)	
56	U	G	U	G	U	A	A	C	3	62.3(±3.0)	
57	A	U	U	U	A	U	A	A	5	61.7(±0.1)	
58	C	G	U	U	U	U	A	A	4	61.5(±4.5)	
59	U	G	U	C	U	U	A	U	3	60.9(±0.8)	
60	C	G	C	U	A	A	A	U	3	60.7(±3.7)	
61	G	U	U	U	A	A	A	U	3	60.1(±1.8)	
62	G	G	U	C	A	A	G	U	2	59.7(±0.9)	
63	G	G	U	C	G	U	C	U	3	59.6(±1.3)	
64	G	G	U	C	G	G	G	U	4	58.7(±2.0)	
65	G	G	A	U	U	U	A	U	4	58.6(±2.0)	
66	U	G	U	A	C	C	A	C	4	58.5(±0.3)	
67	C	G	U	U	C	U	G	U	3	58.2(±1.5)	
68	U	G	U	G	U	A	A	C	3	57.0(±2.5)	
69	A	G	U	G	U	C	A	U	3	56.5(±3.0)	
70	U	G	U	C	G	U	G	C	6	56.4(±3.9)	

71	A	G	U	C	U	C	A	U	4	55.8(±2.4)
72	<u>G</u>	G	U	<u>G</u>	<u>G</u>	<u>C</u>	<u>G</u>	U	3	55.1(±1.0)
73	G	G	<u>G</u>	<u>C</u>	<u>C</u>	<u>U</u>	<u>A</u>	U	4	54.7(±4.2)
74	<u>U</u>	G	<u>U</u>	<u>G</u>	<u>C</u>	<u>U</u>	A	C	4	51.2(±2.7)
75	<u>A</u>	G	U	<u>C</u>	<u>C</u>	<u>C</u>	A	<u>U</u>	4	50.6(±1.4)
76	<u>G</u>	G	<u>C</u>	<u>C</u>	<u>C</u>	<u>C</u>	A	U	4	50.6(±1.3)
77	<u>A</u>	G	<u>C</u>	<u>G</u>	<u>C</u>	<u>A</u>	A	U	3	50.3(±1.5)
78	<u>U</u>	G	<u>U</u>	G	<u>G</u>	<u>U</u>	<u>G</u>	<u>C</u>	5	50.0(±0.9)
79	<u>G</u>	<u>U</u>	<u>A</u>	<u>A</u>	<u>G</u>	<u>A</u>	<u>A</u>	<u>U</u>	4	49.7(±4.3)
80	<u>A</u>	<u>G</u>	<u>U</u>	<u>A</u>	<u>C</u>	<u>A</u>	<u>G</u>	U	4	49.0(±1.9)
81	<u>A</u>	G	U	<u>C</u>	<u>G</u>	<u>C</u>	<u>A</u>	U	4	48.1(±1.4)
82	<u>U</u>	G	U	<u>C</u>	<u>G</u>	<u>C</u>	A	C	5	47.9(±2.3)
83	<u>C</u>	G	U	<u>G</u>	A	<u>U</u>	A	<u>U</u>	3	47.6(±0.4)
84	<u>C</u>	G	<u>U</u>	<u>G</u>	A	<u>U</u>	A	U	2	46.7(±1.3)
85	<u>U</u>	G	U	<u>C</u>	<u>C</u>	<u>C</u>	<u>G</u>	<u>C</u>	6	45.5(±0.2)
86	<u>G</u>	G	<u>C</u>	<u>C</u>	<u>C</u>	<u>A</u>	<u>A</u>	<u>U</u>	3	45.4(±3.7)
87	<u>U</u>	G	<u>U</u>	<u>G</u>	<u>U</u>	<u>U</u>	A	<u>A</u>	4	44.7(±3.5)
88	<u>U</u>	G	U	<u>U</u>	<u>U</u>	<u>U</u>	A	<u>C</u>	5	42.6(±0.1)
89	<u>C</u>	G	U	<u>A</u>	<u>A</u>	<u>C</u>	A	<u>A</u>	3	42.5(±3.9)
90	<u>C</u>	G	U	<u>C</u>	U	<u>A</u>	A	<u>U</u>	3	42.3(±4.2)
91	<u>A</u>	G	U	<u>A</u>	<u>A</u>	<u>A</u>	<u>C</u>	<u>A</u>	4	41.2(±1.8)
92	<u>G</u>	G	U	<u>U</u>	<u>U</u>	<u>C</u>	<u>G</u>	<u>U</u>	4	39.0(±3.7)
93	<u>U</u>	G	U	<u>C</u>	<u>U</u>	<u>U</u>	<u>G</u>	<u>C</u>	6	38.9(±4.5)
94	<u>U</u>	G	U	<u>G</u>	A	<u>U</u>	<u>A</u>	<u>U</u>	2	38.3(±1.2)
95	<u>A</u>	<u>U</u>	A	G	<u>C</u>	<u>U</u>	A	<u>A</u>	5	38.1(±0.6)
96	<u>U</u>	<u>G</u>	U	G	<u>C</u>	<u>C</u>	G	<u>C</u>	5	33.1(±1.9)
97	<u>C</u>	<u>U</u>	U	<u>U</u>	<u>U</u>	<u>A</u>	<u>A</u>	<u>A</u>	5	32.4(±3.7)
98	<u>C</u>	G	<u>C</u>	<u>U</u>	<u>G</u>	<u>U</u>	A	<u>U</u>	4	31.2(±1.4)
99	<u>C</u>	G	<u>U</u>	<u>C</u>	<u>A</u>	<u>G</u>	A	<u>A</u>	4	29.2(±3.3)
100	<u>G</u>	G	U	<u>G</u>	<u>C</u>	<u>C</u>	A	<u>U</u>	2	22.4(±3.0)
101	G	G	<u>G</u>	G	<u>C</u>	<u>C</u>	A	U	3	22.2(±4.2)

<sup>a</sup> Sequences of the 690 loop instant-evolution mutants. The 101 unique sequences are numbered in order of decreasing function. Mutations are underlined.

<sup>b</sup> Number of mutations in each sequence.

<sup>c</sup> GFP activity as a percentage of the wild-type (pRNA123).

<sup>d</sup> Sequence of the unmutated control, pRNA123, (WT, wild-type).

absent at position 691 in the instant-evolution mutants, these substitutions may also affect ribosome function. It should be noted, however, that the frequency with which a particular nucleotide is represented does not depend directly upon the effect of that nucleotide on function. Instead, it reflects the number of random sequences containing that nucleotide that are functional at or above the level required to survive chloramphenicol selection. The mutants containing purine bases at position 690, on average, are 20% more functional than those with pyrimidines. Only three G695-containing mutants were isolated. The average function of these three mutants was 32%. These data suggest that only a small number of sequences in the mutant pool containing G695 are functional. The only substitution of A696 was a transition to G found in 19 out of 101 sequences.

### Covariation analysis

To identify potentially functionally significant nucleotide covariations among the instant-evolution mutants, we examined the distribution of each pair of mutated nucleotides. For this we used the chi-squared ( $\chi^2$ ) contingency test for independence to determine how close the observed nucleotide frequencies were to the expected frequencies if no functional interactions existed. The probability ( $p$ ) that the observed covariation is due to random fluctuations is provided: chi-squared probabilities less than 0.001 ( $\chi^2$ ,  $p < 0.001$ ) are considered statistically significant.

The most significant covariations found in the 690 loop are shown by arrows in Figure 4(a). Positions 690 and 697 showed the most significant covariation ( $\chi^2$ ,  $p = 2.5 \times 10^{-18}$ ), suggesting the existence of a functionally important interaction between nucleotides at these positions (Figure 4(a), unbroken arrow). The G690:U697 pair is highly conserved evolutionarily, with rare occurrences of A690 and no substitutions of U697 in bacterial ribosomes (Table 2). Among the instant-evolution mutants, 59 have a G690:U697 pair. The other most frequently represented combinations between positions 690 and 697 are 15 U:C, six A:A, and ten A:U pairs, suggesting that these mutants share functionally important features with the wild-type G690:U697 pair (see Discussion).

For positions 691 and 696, there were no double mutants, prohibiting meaningful covariation analysis between these two positions. A strong preference for particular pairs with one substitution, however, was observed. Among the instant-evolution mutants, 68 contain the wild-type G691:A696 pair. The other 691:696 isolates are 19 G:G, nine U:A, and five A:A pairs. No other combinations were isolated. Though sequence variation at positions 691 and 696 was too constrained to provide statistically significant covariation, the functional nucleotide pairs obtained in the instant-evolution selection are each capable of forming structures isomorphous with the sheared G·A conformation observed in the NMR structure

**Table 2.** Sequence variation in the 690 loop

Nucleotide	690	691	692	693	694	695	696	697
<b>A. Nucleotide distribution of functional mutants<sup>a</sup></b>								
A	17(8)	5(5)	5(3)	15(10)	<u>26(16)</u>	<u>36(19)</u>	<u>82(46)</u>	11(3)
C	6(0)	0	11(5)	36(17)	<u>22(13)</u>	<u>30(16)</u>	0	16(4)
G	<u>60(40)</u>	<u>87(42)</u>	3(0)	<u>25(9)</u>	25(12)	3(0)	19(5)	0
U	18(3)	9(4)	<u>82(43)</u>	<u>25(15)</u>	28(10)	<u>32(16)</u>	0	<u>74(44)</u>
$\chi^2, p$	$1.6 \times 10^{-14}$ ( $2.8 \times 10^{-17}$ )	$9.8 \times 10^{-44}$ ( $1.7 \times 10^{-19}$ )	$6.2 \times 10^{-37}$ ( $8.0 \times 10^{-21}$ )	$3.3 \times 10^{-2}$ ( $3.2 \times 10^{-1}$ )	$8.6 \times 10^{-1}$ ( $6.9 \times 10^{-1}$ )	$6.2 \times 10^{-6}$ ( $5.7 \times 10^{-4}$ )	$1.1 \times 10^{-38}$ ( $3.6 \times 10^{-25}$ )	$3.6 \times 10^{-28}$ ( $3.9 \times 10^{-22}$ )
<b>B. Nucleotide distribution in all known bacteria<sup>b</sup></b>								
A	297	2	3	266	<u>3277</u>	<u>3744</u>	<u>3750</u>	0
C	2	2	12	3	1	0	0	0
G	<u>3437</u>	<u>3737</u>	1	<u>3383</u>	464	0	0	0
U	3	2	<u>3734</u>	8	0	1	0	<u>3751</u>

<sup>a</sup> Nucleotide distribution of the 690 loop instant-evolution mutants.  $\chi^2, p$  is the probability that the observed distribution occurred as a result of random chance. Parentheses indicate distribution of the subset of 51 mutants with function  $\geq 65\%$ .

<sup>b</sup> Phylogenetic variation of the 690 loop nucleotides in bacterial ribosomes (Van de Peer *et al.*, 1999). Underlined numbers indicate the wild-type *E. coli* sequence.

of the 690 loop (Morosyuk *et al.*, 2001) (see Discussion). Therefore, the covariation between 691 and 696 is shown in Figure 4(a) by a broken arrow.

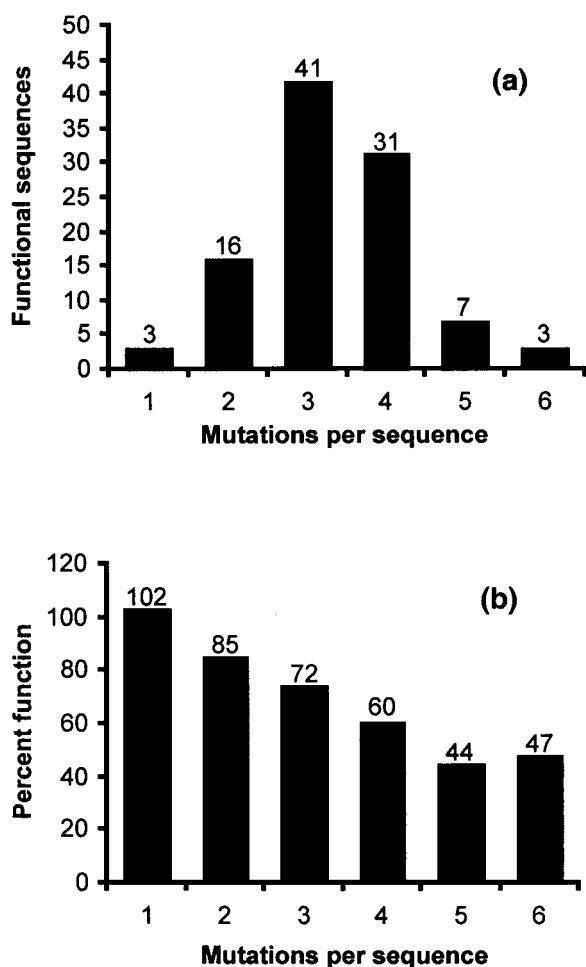


**Figure 3.** Functional analysis of the instant-evolution pool. (a) Mutation distribution, showing the number of clones isolated with the indicated number of mutations. (b) Correlation of function with the number of mutations per clone.

We also found three weak ( $p > 0.01$ ) covariations in the loop between positions 691 and 695 ( $\chi^2, p = 0.05$ ), between positions 692 and 695 ( $\chi^2, p = 0.04$ ), and between positions 694 and 696 ( $\chi^2, p = 0.04$ ). The 691:695 pair, however, had only five double mutants, which is not sufficient to draw a definitive conclusion about covariation. Positions 693 and 694 showed no covariation with any other mutated position in the loop. These covariations appear to be due to selection against stable pairing combinations between positions 692 and 695 that would disrupt functionally important interactions such as the 691-696 mismatch (see Discussion).

#### Site-directed mutagenesis of the 690:697 and 691:696 base-pairs

Analysis of the instant-evolution mutants suggested the existence of functionally important interactions between G690 and U697 and between G691 and A696. In addition, nucleotide variation at three of these positions, 690, 697, and 696, correlates with ribosome function (Figure 4(a)). To examine the nature of the functional constraints at these positions more closely, we used site-directed mutagenesis to construct all 15 nucleotide combinations between positions 690 and 697 and between 691 and 696 without changing other nucleotides in the 690 loop. Functional data for the 690:697 and 691:696 mutants are consistent with the analyses of the instant-evolution mutants and are summarized in Figures 5 and 6, respectively.

Ribosome function in the 690:697 mutants varied from 22.4% (C:G) to 89% (A:U) of the control (Figure 5). Each of the single and double mutants with functions greater than 45% of the wild-type was represented at least once in the pool of instant-evolution mutants. Mutants with functions less than 45% were excluded from the instant-evolution pool. Out of 15 site-directed mutants of the 690:697 pair, the G690:C697 (30.5%) and C690:G697 (22.4%) pairs have the lowest function, indicating that formation of a strong Watson-Crick

base-pair between positions 690 and 697 inhibits ribosome function.

The 691:696 site-directed mutants show a very different functional profile from the 690:697 pair mutants (Figure 6). Only three single mutants retained a significant level of function, A691:A697 (94.1%), U691:A691 (88%), and G691:G696 (87.8%). These three mutants were also the only variants of the 691:696 pair isolated in the instant-evolution mutants, providing further evidence that these nucleotide pairs share functionally important features with the wild-type sheared G691:A696 pair observed in the NMR structure (see Discussion). All of the other site-directed mutants at positions 691 and 696 produced ribosomes that were less than 25% as functional as the wild-type. The double pyrimidine-pyrimidine mutants were all less than 5% as functional as the control.

## Discussion

### Instant-evolution versus phylogeny

Here, we use instant evolution to identify functionally significant nucleotides and nucleotide interactions within the conserved 690 loop of *E. coli* 16 S rRNA. Sequence analysis revealed more variability in the instant-evolution mutants than observed in phylogenetic ribosomal RNA databases (Table 2). Instant-evolution experiments identify the major factors affecting function in a defined RNA sequence. Both the system and the selection scheme were designed to allow isolation of suboptimal sequences. Therefore, it is likely that the greater variability observed among the instant-evolution mutants when compared with phylogenetic databases is due to the relaxed functional constraints imposed during selection of the instant-evolution mutants. By correlating nucleotide variation with GFP production in the instant-evolution pool, we identified individual nucleotides and nucleotide interactions that are important for ribosome function.

Substitution patterns in the instant-evolution mutants were similar to those observed in nature at all positions except 693, 694 and 695, which showed very little or no nucleotide preference or correlation of nucleotide identity with ribosome function (Tables 2 and 3). Purine bases are strongly preferred at positions 693 and 694 among naturally occurring ribosomes, but in the instant-evolution mutants all four nucleotides are equally represented. In addition, no correlation between nucleotide identity and ribosome function was observed at these positions. In the accompanying paper (Morosyuk *et al.*, 2001), the NMR structure shows that nucleotides 692-695 form a U-turn motif (Figure 4(b)) closed by a sheared G691·A696 pair, consistent with the definition for a classic U-turn with UNR consensus sequence closed by a mismatch with sheared geometry (Gutell *et al.*, 2000). More than 99% of naturally occurring 690 loop sequences are consistent with the U-turn

motif (Gutell *et al.*, 2000). Other RNA hexaloops also form structures that share many similar features with the 690 loop including the G·A sheared pair, the U-turn, and stacking of the nucleotides in the minor groove. Two examples are the GUAAUA loop sequence of the L11 binding site in the 23 S rRNA (Fountain *et al.*, 1996; Huang *et al.*, 1996) and the GUAACA sequence of the loop IIa from U2 snRNA (Stallings & Moore, 1997). It is interesting that both of these sequences are found among the 690 loop instant-evolution mutants (Table 1, sequences 41 and 38, respectively). Nucleotide U692 in the 690 loop appears to be phylogenetically conserved because it forms favorable stacking interactions and has an imino group for hydrogen bonding with the phosphate backbone across the loop. G and C have also been shown to facilitate turning of the phosphate backbone in RNA in a U-turn motif (Jucker *et al.*, 1996; Su *et al.*, 1999). Under the relaxed constraints of the instant-evolution experiment, however, 55 sequences were isolated that do not strictly adhere to the UNR motif. Eight sequences have a purine at position 692 and 50 sequences have a pyrimidine at position 694. By comparing our structural data with the instant-evolution analyses, we conclude that nucleotides 692-695 must form a turn at the top of the loop but that these nucleotides need not adhere to the UNR motif. The functional significance of the 690 U-turn is discussed below.

All naturally occurring bacterial sequences except one (U) contain an A at position 695. The instant-evolution pool contained only three A695G mutants with an average function of 32% (Tables 2 and 3). Approximately equal numbers of mutants containing A, C, and U at position 695 were isolated. The X-ray structure reported by Wimberly *et al.* places the A695-N1 within H-bonding distance (3.3 Å) of G786-N2; an interaction that would be disrupted by A695G substitution, which would place two H-bond donors in close proximity (Wimberly *et al.*, 2000). Weak covariations were observed between position 695 and positions 691 and 692 (Figure 4). It is possible that G at position 695 was selected against among the instant-evolution mutants because it hydrogen bonds with other nucleotides and disrupts the functional conformation of the loop. Similar patterns were observed among the instant-evolution mutants at positions 792 and 793 of 16 S rRNA (Lee *et al.*, 1997).

### Structure versus function

It is difficult to separate structure from function in catalytic RNAs because even single-nucleotide changes may alter the structure of an RNA molecule enough to cause large changes in function. Multiple compensatory mutations, however, may preserve the active form. Since single structural mutations often cause significant loss of function, compensatory mutations must occur simultaneously in nature and are therefore extremely rare. As a result, the conserved, functionally

**Table 3.** Mean activity of mutations at each position

Nucleotide	690	691	692	693	694	695	696	697
A	61.8	76.9	71.5	75.8	<u>71.8</u>	72	<u>71.6</u>	53.3
C	43.3	n/a	65.1	68.9	<u>72</u>	69.8	n/a	55.3
G	<u>77.7</u>	<u>68.5</u>	47	<u>60.8</u>	65.4	32	55.8	n/a
U	53.2	64.9	<u>69.7</u>	71.8	65.9	67.1	n/a	<u>73.9</u>
$p^a$	$5.2 \times 10^{-6}$	0.7	0.4	0.2	0.6	0.04	0.009	0.001

Mean GFP activity of all instant-evolution mutants with the indicated nucleotide at each position. Underlined numbers indicate the wild-type nucleotide.

<sup>a</sup> The  $p$ -value, the probability that the observed differences in function are unrelated to nucleotide identity as measured by single-factor analysis of variance (ANOVA).

important nucleotides in ribosomal RNA are often located among equally conserved nucleotides whose role is primarily structural. In instant-evolution experiments, all of the nucleotides in a particular region are simultaneously mutated and only functional sequences are isolated. Because these sequences are selected for sub-optimal levels of function, alternative nucleotide combinations among structurally important positions are isolated. Nucleotides directly involved in function, such as those involved in intermolecular interactions, however, generally show little variation (Lee *et al.*, 1997). Comparison of sequence variation patterns among the instant-evolution mutants allows identification of structurally important

nucleotide motifs. Thus, one application of instant-evolution is to provide functional significance for the structural motifs observed in NMR and X-ray crystallographic structures. Here, we correlate instant-evolution function with the NMR solution structure of the 690 loop to identify the key structural elements required for function (Figure 4).

#### Functional significance of G690·U697

A highly significant covariation was observed between positions 690 and 697 (Figure 4(a)), suggesting the existence of a functional interaction between these two nucleotides. These findings are consistent with our previous instant-evolution stu-

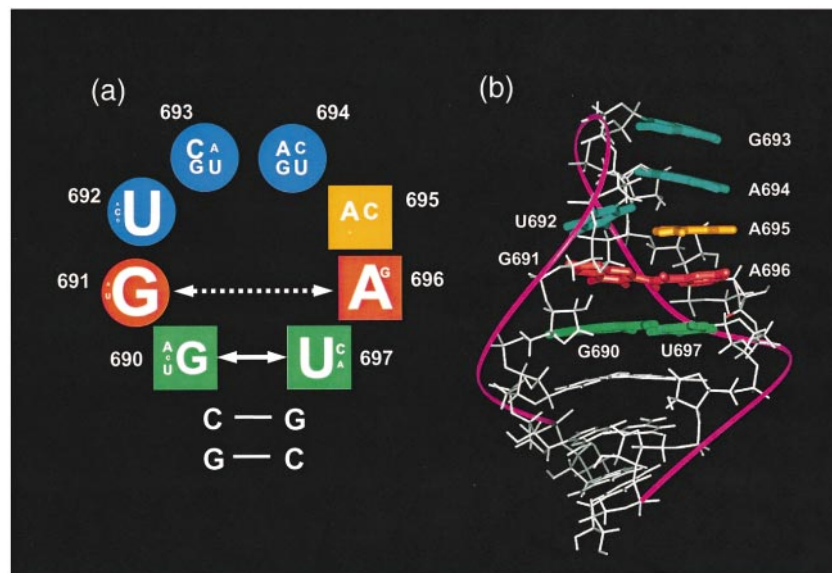


**Figure 4.** The 690 loop structure and function. (a) Summary of sequence and covariation analysis of the 690 loop instant-evolution mutants. Nucleotide font size at each mutated position in the loop is proportional to the occurrence of this base in the 101 instant-evolution mutants (Table 2A). Positions that show a significant correlation between level of function and nucleotide identity are boxed. The significant covariation observed between position 690 and 697 ( $p = 2.5 \times 10^{-18}$ ) is indicated by the unbroken arrow. The proposed covariation between 691 and 696 is shown by a broken arrow. Only the covariations with  $p < 0.001$  are shown. We also found three weak covariations in the loop, between positions 691 and 695 ( $\chi^2$ ,  $p = 0.05$ ), 692 and 695 ( $\chi^2$ ,  $p = 0.04$ ), and 694 and 696 ( $\chi^2$ ,  $p = 0.04$ ). (b) The NMR solution structure of the 690 loop (Morosyuk *et al.* 2000, 2001). The nucleotides from 693 to 697 form an array of stacked bases in the minor groove of the 690 loop with the Watson-Crick functional groups available for interactions. The U-turn of the phosphate backbone occurs between U692 and G693. Two sheared mismatches are formed at the base of the loop between G690 and U697 and between G691 and A696. (b) NMR solution structure of the 690 loop. Different structural motifs found in the NMR structure are color-coded. The green pair is the sheared single H-bond G690·U697 mismatch, the red pair is the sheared G691·A696 mismatch, the blue nucleotides form the U692-G693-A694 U-turn, and the A695 nucleotide stacked in the minor groove is yellow.

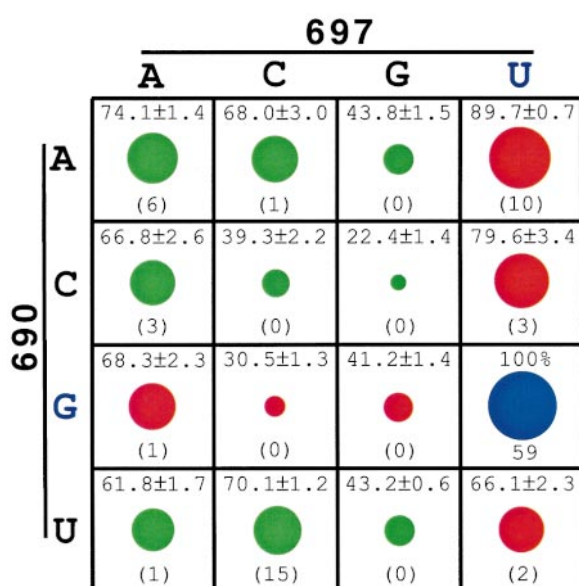


**Figure 5.** Functional analysis of the 690:697 site-directed mutants. The wild-type blue is (G690:U697), double mutants are green, and single mutants are red. The size of the dots is proportional to the level of function as compared to the wild-type. The mean function (percentage of the wild-type) of three GFP assays is provided at the top of each box with the standard error. Numbers in the parentheses indicate the occurrence of the corresponding nucleotide pair among the instant-evolution mutants. All 690:697 mutant pairs with the level of function below 60% were absent in the instant-evolution pool.

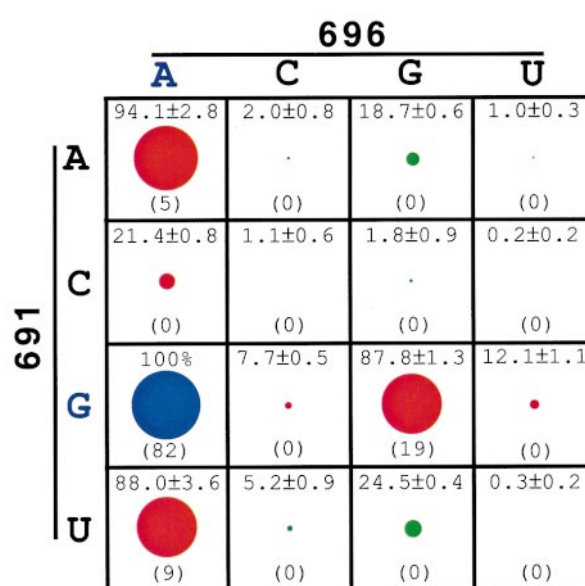


**Figure 6.** Functional analysis of the 691:696 site-directed mutants. The wild-type blue is (G691:A696), double mutants are green, and single mutants are red. The size of the dots is proportional to the level of function as compared to the wild-type. The mean function (percentage of the wild-type) of three GFP assays is provided at the top of each box with the standard error. Numbers in the parentheses indicate the occurrence of the corresponding nucleotide pair among the instant-evolution mutants. Only three single mutants retain significant function (A691:A696, U691:A696, and G691:G696).

dies of the 690 stem nucleotides (Morosyuk *et al.*, 2000). At position 690, G is conserved with rare occurrences of A690 among naturally occurring bacterial ribosomal RNA sequences and U697 is invariant among bacterial ribosomes (Table 2). The 690 loop NMR solution structure revealed a novel sheared type G690·U697 mismatch (Morosyuk *et al.*, 2001). To determine the functional significance of this novel structural motif, we examined the effect of each 690:697 mutant pair among the instant-evolution mutants on GFP synthesis *in vivo*. Among the 51 instant-evolution mutants with function  $\geq 65\%$  of the wild-type (Tables 2 and 3), 40 are G·U (average function = 91%), four are A·U (75%), three are A·A (78%), three are U·C (69%), and one is A·C (66%). Each of these mutant pairs is able to form a structure isomorphous with the sheared G·U observed in the 690 NMR solution structure (Figure 7) (Auffinger & Westhof, 1999), suggesting that the sheared conformation is required for function. An alternative explanation is that the sheared conformation facilitates proper placement of an essential functional group either in the 690-697 pair or elsewhere in the loop. In the crystal structure reported by Wimberly *et al.* (2000) a hydrogen bond was observed between the O2 of U697 and the NH<sub>2</sub> of G785.

To further examine the 690-697 interaction, we constructed and analyzed all 15 mutant combinations at positions 690 and 697 (Figure 5). If the sheared conformation is important for ribosome function, the site-directed mutants able to form structures isomorphous with the sheared G·U observed in the NMR structure should be more functional than those unable to form isomorphous structures. On the other hand, if proper placement of an H-bond acceptor at position 697 is the critical functional determinant, then combinations that either do not have an H-bond acceptor or that produce a structure where the H-bond acceptor cannot access the NH<sub>2</sub> of G785 should have low function.

Based on current literature, nucleotide pairs predicted to form isomorphous structures with the sheared G·U are A·A, U·C, G·A, C·A, A·C, U·A, C·C and G·G as shown in Figures 7 and 8 (Auffinger & Westhof, 1999; Batey *et al.*, 2000; Leontis & Westhof, 1998a,b). The functional data for each of the 16 site-directed mutants are shown in Figure 5. The order of function of the site-directed mutants is G·U > A·U > C·U > A·A > U·C > G·A > A·C > U·A > U·U > U·A  $\gg$  A·G > U·G > G·G > C·CC  $\gg$  G·C  $\gg$  C·G. The predicted isomorphous pairs are the most functional of the site-directed mutants with the exceptions of C·C and G·G, which are only 39% and 41% as functional as the wild-type. We

showed previously that proper pairing among the 690 stem nucleotides is essential for ribosome function (Morosyuk *et al.*, 2000). Secondary structure predictions (mfold) (Zuker, 1989) of the C690:C697 site-directed mutant show the formation of a non-functional secondary structure in which C690 is paired with G700 and C697 is paired with G693. The stability of the predicted structure is  $-2.2$  kcal/mol more stable than the functionally active structure in which G688 is paired with C699 (Morosyuk *et al.*, 2000). Therefore, the C·C site-directed mutant is probably less functional than expected because it permits formation of a nonfunctional secondary structure in the 690 hairpin. The 690·697 site-directed mutants, A·C, A·U, C·U, and U·U, however, all show greater function than expected since these pairs have not previously been predicted to assume a conformation isomorphous with the sheared G·U observed in our NMR structure. As shown in Figure 7, however, A·C can form an isomorphous sheared pair stabilized by a single hydrogen bond. The high level of function observed for A·U, C·U, and U·U suggests that even though they cannot form hydrogen bonds in the sheared conformation they can form structures *in vivo* that place the U697-O2 functional group in a position where it is available for interaction with G785. Therefore, though most of the functional pairs in the instant-evolution and site-directed mutants are able to form structures isomorphous with the sheared G·U observed in our NMR structure, it is likely that this is because a hydrogen bond is required between G785-NH<sub>2</sub> and an appropriately positioned H-bond acceptor at position 697.

Comparison of the functional and non-functional 690·697 nucleotide pairs shows that those with a G at 697 have low activity while those with A, C, and U are  $>65\%$  as functional as the wild-type. Each of the predicted structures formed by isomorphous replacement of U697 with A or C contains a hydrogen-bond acceptor in the minor groove of the 690 stem (Figure 4). Substitution of G at position 697, however, would place a hydrogen-bond donor (amino) in the corresponding position, which would require structural perturbation to interact with G785. This may explain why the G690·G697 mutant is less functional than expected.

#### Functional significance of the G691·A696 mismatch

Among the bacteria, G691 is found in all but six sequences and A696 is universally conserved (Table 2). In our NMR structure A696 stacks between A695 and U697 and forms a sheared pair with G691. In addition, in the Wimberly *et al.* (2000) structure, N1 and N6 of A696 form two hydrogen bonds to the 2'-OH of C797. In spite of the relaxed functional constraints imposed by instant-evolution selection, very little sequence variation was obtained at positions 691 and 696 (Figure 4(a)). Though lack of double mutations at positions 691 and 696 prohibited meaningful covariation analysis, strong preferences for particular

pairs containing single mutations were observed. Among the 51 instant-evolution mutants with function  $\geq 65\%$  of the wild-type (Tables 1 and 2), 37 are G·A (average function = 91%), five are A·A (77%), four are U·A (85%), and five are G·G (70%). Three features are shared by these 691-696 functional isolates: (1) they are all capable of forming a sheared geometry (Figure 8); (2) they all contain a purine at position 696 that would promote stable stacking interactions with A695 and U697; and (3) they are all able to form hydrogen bonds to the 2'-OH of C797.

Since so little variability between positions 691 and 696 was observed among the instant-evolution mutants, all nucleotide combinations were constructed by site-directed mutagenesis and assayed for function (Figure 6). As with the 690:697 mutants, if the three common features identified for the 691·696 pairs isolated in the instant-evolution pool are important for ribosome function, site-directed mutants possessing these features should be more functional than those without them. The functional data for each of the 15 site-directed mutants is shown in Figure 6. The mutants fall into three functional classes: the class I mutants (UA, GG and AA) all had near wild-type function, (mean activity = 90%); class II mutants (UG, CA and AG) had low function (22%) and the remaining mutants (class III) were non-functional (3%).

All of the mutants in class I contain a purine at position 696, are able to assume the sheared geometry, and are all able to form hydrogen bonds to the 2'-OH of C797. The class II mutants all contained a purine at position 696, but are unlikely to form sheared pairs. Based on current literature, nucleotide pairs predicted to form isomorphous structures with the sheared G·A are G·U, A·A, U·C, C·A, A·C, U·A, G·G and C·C as shown in Figures 7 and 8 (Auffinger & Westhof, 1999; Batey *et al.*, 2000; Leontis & Westhof, 1998a,b; Morosyuk *et al.*, 2001). Three of the 691·696 pairs (U·C, C·C, and C·A) produced ribosomes with significantly lower function than expected (Figure 7). Secondary structure analysis (mfold) of these site-directed mutants predicts formation of non-functional secondary structures in which position 691 is paired with G698. The predicted structures are  $-1.4$  to  $-4.8$  kcal/mol more stable than the functionally active structure. Therefore, the U·C, C·C, and C·A site-directed mutants probably form non-functional secondary structures in the 690 hairpin *in vivo*. This is consistent with the low function observed in the C·A mutant even though it contains a purine at position 696, since it is unlikely that the resulting secondary structure permits H-bond formation from A696 to C797. The only class III mutant with a purine in positions 696 (C·G) cannot form a sheared pair and is most likely to form a Watson-Crick pair. The resulting structure would disrupt the stacking interactions observed in this region of the 690 loop and prevent H-bond formation with C797.

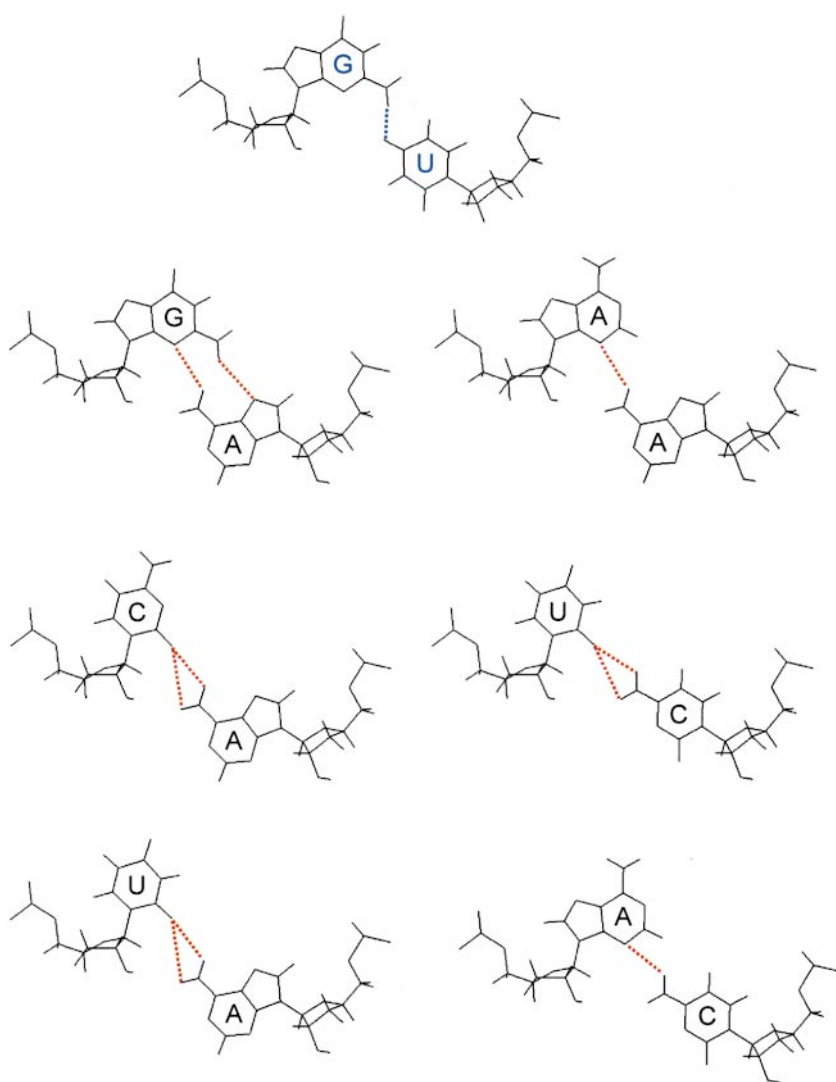


**Figure 7.** Isomorphous substitutions at positions 690 and 697. Mutant nucleotide pairs were modeled into the 690·697 G·U NMR mismatch structure using the Builder module of Biosym InsightII without energy minimization. Each of these mutant pairs is able to form hydrogen-bonding interactions isomorphous with the sheared G690·U697 observed in the NMR structure. Similar isosteric sheared pairs were observed previously in tRNA positions 32-38 for A·A, G·A, C·A, U·C and U·A (Auffinger & Westhof, 1999). An isosteric sheared pair similar to the A·C pair shown was proposed based on phylogenetic variation at positions A72·C104 in 5 S rRNA (Leontis & Westhof, 1998a).

The instant-evolution data suggest that certain pairs of nucleotides inhibit ribosome function by disrupting some essential structural feature of the 690 loop. We compared function in each of the site-directed double mutants with the corresponding single mutants (Table 4). Functional activity in double mutants should be approximately equal to the product of the functional activities of each of the corresponding single mutants if the two mutation sites do not interact. As shown in Table 4, each of the double mutants is less functional than would be predicted if they were independent. Therefore, functional analysis of the 691·696 single mutants A·A (94.1%) and G·G (87.8%) predicts that the function of the A·G double mutant would be 82.6% if no interaction occurred between nucleotides at these positions. The actual function of the A·G double mutant, however, is 18.7%. Similar patterns are observed for all of the 691·696 double mutants, suggesting that formation of an incorrect interaction inhibits ribosome function since none of the double mutants that form the correct secondary structure is capable of forming a sheared pair isomorphous with G·A. Since each of

the functional 691·696 pairs can form a sheared structure (Figure 8) that contains a purine at position 696, we conclude that these two features are required for ribosome function. In the NMR structure, nearly ideal stacking of the sheared G690·U697 and G691·A696 pairs is observed (Figure 4(b)) (Morosyuk *et al.*, 2001). These data suggest that G691·A696 in combination with G690·U697 form a structure that is essential for ribosome function.

#### Functional significance of the U-turn

As shown by our 690 NMR structure, the wild-type sequence of the 690 loop folds into a structure similar to the anticodon loop of tRNA as well as several other RNAs that participate in receptor interactions (Auffinger & Westhof, 1999; Morosyuk *et al.*, 2001; Pley *et al.*, 1994; Stallings & Moore, 1997). In addition, the phylogenetic data for the tRNA anticodon stem (Figure 9) resemble our instant-evolution data for the 690 loop (Figure 4(a)). Each of these RNAs shares the common motifs of a closing sheared pair, stacked nucleotides on the 3'

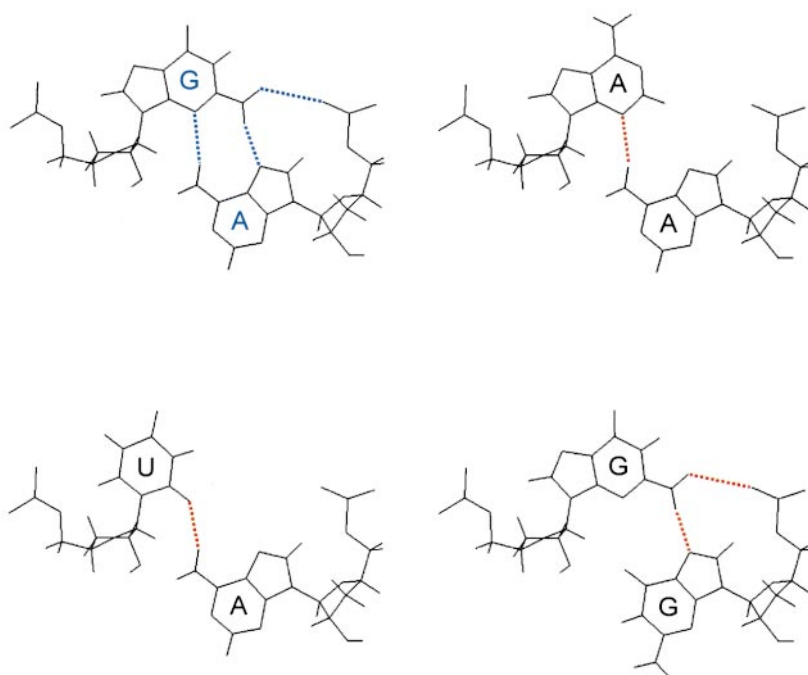


**Figure 8.** Isomorphous substitutions at positions 691 and 696. Mutant nucleotide pairs were modeled into the 691·696 G·A NMR mismatch structure using the Builder module of Biosym InsightII without energy minimization. Each of these mutant pairs is able to form hydrogen-bonding interactions isomorphous with the sheared G691·A696 observed in the NMR structure. Structures similar to those shown for G·A, A·A and U·A have been previously observed in X-ray crystal structures (Auffinger & Westhof, 1999). A sheared mismatch structure similar to the predicted G691·G696 mismatch is observed in the SRP crystal structure, which has a hydrogen bond from G162-N2 to G149-O6 (2.81 Å) and a somewhat longer distance to G149-N7 (3.56 Å) (Batey *et al.*, 2000).

side of the loop, and a U-turn. In the wild-type sequence, G693 is located at the top of the loop, stacked upon A694 with its functional groups exposed to solvent (Figure 4). A number of studies have implicated this residue in ribosome function. Nucleotide 32 in the anticodon loops of both P-site and E-site bound tRNAs crosslink with G693 in 16 S RNA (Doring *et al.*, 1994). In addition, G693 is protected from kethoxal modification by P-site bound tRNA (Moazed & Noller, 1986, 1990). Kethoxal modification of G693, however, does not prevent P-site tRNA binding (von Ahlsen & Noller, 1995). Nucleotides in the 690 loop were also identified as targets for cleavage by P-site bound anticodon stem loops derivatized with EDTA-Fe(II) (Joseph *et al.*, 1997). These authors speculated that the 690 loop and the 790 loop in the 30 S subunit are positioned such that they would block translocation of tRNA from the P site to the E site and that these loops may have to move as the tRNA shifts from the P site to the E site. These data suggest that G693 either binds to tRNA in the P site or binds to another portion of the translational machinery upon tRNA binding to the P site. The X-ray structure of the 30 S subunit suggests that a stacking interaction forms between G693 and the 5' nucleotide of the E site codon of mRNA.

No nucleotide preference was observed at position 693 among the instant-evolution mutants (Table 2A), though G693 is phylogenetically highly conserved (Table 2B). Interestingly, position 693 was mutated in all of the ten instant-evolution isolates with function greater than that of the wild-type (Table 1). One of these mutants (Table 1, sequence 2) contained a single G693U substitution but produced 22% more GFP than the wild-type. Therefore, mutations at position 693 do not prevent tRNA binding to the P site, but instead appear to

increase the rate of protein synthesis. These data are consistent with modification interference experiments showing that kethoxal modification of G693 does not prevent tRNA binding to the ribosomal P site (von Ahlsen & Noller, 1995). In the 30 S structure reported by Wimberly *et al.* (2000) G693 is stacked on the 5' base of the E-site codon in an mRNA analog. Although our data provide no insight as to the mechanism for the observed increase in protein synthesis, it is possible that mutations at position 693 decrease ribosome affinity for tRNA or affect subunit association, since both of these activities have been associated with the 690 hairpin.

The inverse relationship between protein synthesis rate and error rate has been known for some time (Allen & Noller, 1989, 1991; Dong & Kurland, 1995; Gorini, 1971; Ninio, 1974; Pettersson & Kurland, 1980; Thompson & Karim, 1982). Mutations resulting in increased protein synthesis rates but reduced fidelity have been described in both rRNA and ribosomal proteins (Alksne *et al.*, 1993; O'Connor *et al.*, 1992; Piepersberg *et al.*, 1979; Pinard *et al.*, 1994). In our system, mutated ribosomes translate only the CAT and GFP mRNAs. Because both CAT and GFP are relatively small proteins, even a tenfold decrease in translational fidelity would probably be undetectable by GFP assay. A 20% increase in GFP production, however, is easily detectable. In normal cells, ribosomes must translate thousands of mRNAs and minor changes in error rate are more likely to affect cell viability (Ruusala *et al.*, 1984). This may explain why G693 is conserved among naturally occurring rRNA sequences but is highly variable among the instant-evolution mutants.

## Conclusions

The data presented here indicate the existence of two functionally important regions in the 690 hairpin of ribosomal RNA. The base of the loop forms the structural core of the molecule and is defined by a novel sheared G690·U697 mismatch and a sheared G691·A696 mismatch. The sheared conformation was shown by instant-evolution and site-directed mutagenesis studies to be functionally important for proper placement of nucleotide func-

**Table 4.** Analysis of 691:696 double mutants

Mutation			Percent function	
691	696	(wt)	observed <sup>b</sup>	predicted <sup>c</sup>
G	A	(wt)	100.0	
C	A		21.4	
G	G		87.8	
C	G		1.8	18.8
U	A		88.0	
G	C		7.7	
U	C		5.2	6.8
A	A		94.1	
G	C		7.7	
A	C		2.0	7.2
A	A		94.1	
G	G		87.8	
A	G		18.7	82.6
A	A		94.1	
G	U		12.1	
A	U		1.0	11.4
C	A		21.4	
G	C		7.7	
C	C		1.1	1.6
C	A		21.4	
G	C		7.7	
C	U		0.2	1.6
U	A		88.0	
G	G		87.8	
U	G		24.5	77.3
U	A		88.0	
G	U		12.1	
U	U		0.3	10.6

Mutant nucleotides are in red and wild-type nucleotides are in black.

<sup>a</sup> GFP assay results are presented as a percentage of the wild-type.

<sup>b</sup> Predicted function for each double mutant is the product of the functions of the corresponding single mutants. Functional interactions between positions are indicated by different observed and predicted values in the double mutants.

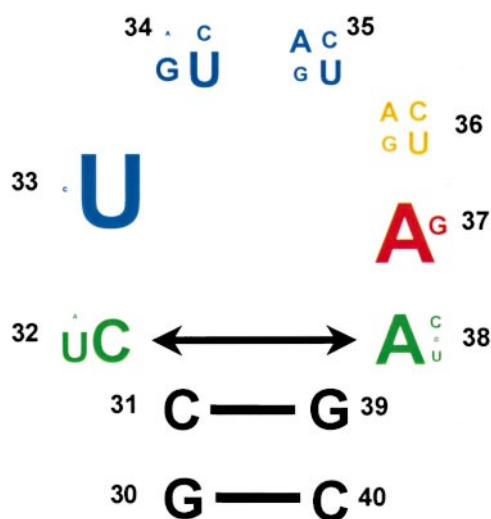


**Figure 9.** Phylogenetic conservation of the tRNA anticodon stem. Positions are color coded to match the corresponding positions in the 690 loop and the closing pair is indicated with an arrow (Figure 4(a) see also, Morosyuk *et al.* 2001, Figure 9). The nucleotide font size at each position in the loop is proportional to the occurrence of this nucleotide in the phylogenetic database (Auffinger & Westhof, 1999).

tional groups involved in interactions with other parts of the translational machinery. The contiguously stacked G693 to U697 residues interact with ribosomal protein S11 and nucleotides in the 790 stem and are protected from hydroxyl radical cleavage by subunit association (Merryman *et al.*, 1999). Cate *et al.* (1999) identified an intersubunit bridge B7 involving an interaction between the minor groove of the 690 hairpin and the adjacent internal loop of 16 S rRNA and domain IV of 23 S rRNA. Several studies suggest that the 690 region and the adjacent internal loop undergo structural rearrangement during protein synthesis (Agrawal *et al.*, 1998; Joseph *et al.*, 1997; McCutcheon *et al.*, 1999; Moazed & Noller, 1989; Mueller *et al.*, 1997; Stark *et al.*, 1997). All of our mutants with increased translation rates contained a mutation at position 693. In our NMR structure, G693 is located at the apex of the 690 loop and in the crystal structure, G693 stacks on an mRNA analogue in the E site. Taken together, these data suggest that the 690 hairpin is a key component of a conformational switch that occurs during 70 S formation and/or during translocation. The mutational data presented here reveal a number of structural motifs that correlate with ribosome function through the correct placement of specific functional groups that appear to be required for interaction with other parts of the translational machinery. These structure/function models are being tested by genetic complementation studies and structure determination of specific rRNA mutants.

## Materials and Methods

### Reagents

Restriction enzymes, ligase, and calf intestine alkaline phosphatase were from New England Biolabs (Beverly, MA, and from Life Technologies (Bethesda, MD). DNA sequencing was performed in-house with a Li-Cor (Lincoln, NE) Global IR<sup>2</sup> DNA sequencer. Sequencing enzymes, nucleotides, and sequencing buffers were from Epicentre Technologies (Madison, WI). Oligonucleotides were either purchased from Life Technologies or synthesized in-house using a Beckman Oligo 1000 DNA synthesizer. Amplitaq DNA polymerase and PCR reagents were from PE-Biosystems.

### Plasmids

Construction of pRNA123 and pRNA16ST will be described elsewhere. The plasmid pRNA123 was derived from pRNA122 (Lee *et al.*, 1996, 1997) by subcloning the green fluorescent protein (GFP) gene into pRNA122. In this vector, (CAT) mRNA and the GFP mRNA (Chalfie *et al.*, 1994) are translated only by plasmid-derived ribosomes. The CAT protein renders cells resistant to chloramphenicol and is used to select functional mutants. GFP allows rapid and accurate determination of ribosome function by measuring fluorescence directly in whole cells. As in pRNA122, the ribosomal RNA operon is under transcriptional regulation of the *lacUV5* promoter (Brosius *et al.*, 1981). The pRNA16ST construct is similar to pRNA122 but the 23 S rRNA gene has been deleted to provide more unique restriction sites in the 16 S RNA gene.

### Bacterial strains and media

All plasmids were maintained and expressed in *E. coli* DH5 (*supE44*, *hsdR17*, *recA1*, *endA1*, *gyrA96*, *thi-1*, *relA1*) (Hanahan, 1983). Cultures were grown in LB medium (Luria & Burrous, 1957) or LB medium containing 100 µg/ml ampicillin (LB-Amp100). To induce synthesis of plasmid-derived rRNA from the *lacUV5* promoter, IPTG was added to a final concentration of 1 mM. Strains were transformed by electroporation (Dower *et al.*, 1988) using a Gibco-BRL Cell Electroporator. Transformants were grown in SOC medium (Hanahan, 1983) for one hour prior to plating on selective medium to allow expression of plasmid-derived genes.

### Random mutagenesis and selection

All PCR-directed mutagenesis experiments (Higuchi, 1989) were performed by subcloning the PCR-amplified DNA into pRNA16ST using the unique *Bgl*III and *Sac*II restriction sites. The PCR upper primer, 690N-697N, was 5'-CGGTATTCCTCCAGATCTCTACGCNNNNNNNNGCTACACCTGGAATTCTA-3' (N = A, T, C, and G) and the lower primer, 16S-AvrII, was 5'-ACGTCGCAAGACCAAAGAGG-3'. The upper and lower primers were designed to bind to the *Bgl*III restriction site and outside of the *Sac*II restriction site, respectively. The library of random mutants in pRNA16ST was then cloned into pRNA123 using *Bst*EII. Transformants were incubated in SOC medium containing 1 mM IPTG for three hours to induce rRNA synthesis and then plated on LB-Amp100 agar with and without 200 µg/ml chloramphenicol. The minimal inhibitory concentration (MIC) of chloramphenicol for cells expressing wild-type rRNA from pRNA123 plasmid is approximately 650 µg/ml. A total of 500,000

transformants were obtained yielding approximately one chloramphenicol-resistant transformant per 2500 transformants plated. From the chloramphenicol selection plates, 186 survivors were randomly selected, subcultured and sequenced between the *Bgl*III and *Sac*II ligation sites to identify the mutations and to verify the absence of unprogrammed mutations in the PCR products.

### Site-directed mutagenesis of nucleotides at positions 690, 697, 691 and 696

All possible single and double mutants of the 690:697 pair, and the 691:696 pair were constructed first in pRNA16ST using unique *Bgl*III and *Sac*II restriction sites and then cloned to pRNA123 using *Bst*EII. Each set of mutations was constructed using a single mutagenic primer. The mutagenic PCR primer for the 690:697 mutants was 5'-CGGTATTCCTCCAGATCTCTACGCNNTTTCACNGCTACACCTGGAATTCTA-3' and for the 691:696 mutants was 5'-CGGTATTCCTCCAGATCTCTACGCANTTCANCGCTACACCTGGAATTCTA-3'. *E. coli* DH5 cells were transformed with the mutated plasmids and transformants were selected on LB agar plates containing ampicillin (100 µg/ml). The mutations were identified by sequence analysis of plasmids isolated from the transformants.

### GFP assays

Overnight cultures were diluted 1:1000 in LB-Amp100 medium and grown at 37°C with shaking until  $A_{600} = 0.1$ . IPTG was then added to a final concentration of 1 mM and incubated with shaking for an additional three hours. Following incubation, 1 ml of each culture was removed for assay, the cells were pelleted, washed twice in 1 ml of HN buffer (20 mM Hepes (pH 7.4) and 0.85% NaCl), and resuspended in 1 ml of the HN buffer. Cell density ( $A_{600}$ ) was determined using a SPECTRAMax 190 microplate spectrophotometer (Molecular Devices, Sunnyvale, CA) and fluorescence (excitation = 395 nm, emission = 509 nm) was measured using a SPECTRAMax GEMINI microplate fluorometer (Molecular Devices, Sunnyvale, CA). For each culture, fluorescence was divided by  $A_{600}$  and presented as a percentage of the wild-type. Values represent the average of at least three assays on three separate cultures.

## Acknowledgements

We thank Robin Gutell, Allen Nicholson and Jack Parker for helpful discussions, and Christine Chow for oligo synthesis and helpful discussions. We also thank Kris Ann Baker, Laurie Boore, Ashesh Saraiya, Tonya Faulk and Marny Waddington for critical review of the manuscript. This work was supported by NIH grants GM55745 and GM52896.

## References

- Agalarov, S. C. & Williamson, J. R. (2000). A hierarchy of RNA subdomains in assembly of the central domain of the 30 S ribosomal subunit. *RNA*, **6**, 402-408.
- Agrawal, R. K., Penczek, P., Grassucci, R. A. & Frank, J. (1998). Visualization of elongation factor G on the *Escherichia coli*: 70 S ribosome: the mechanism of translocation. *Proc. Natl Acad. Sci. USA*, **95**, 6134-6138.

- Alksne, L. E., Anthony, R. A., Liebman, S. W. & Warner, J. R. (1993). An accuracy center in the ribosome conserved over 2 billion years. *Proc. Natl Acad. Sci. USA*, **90**, 9538-9541.
- Allen, P. N. & Noller, H. F. (1989). Mutations in ribosomal proteins S4 and S12 influence the higher order structure of 16 S ribosomal RNA. *J. Mol. Biol.* **208**, 457-468.
- Allen, P. N. & Noller, H. F. (1991). A single base substitution in 16S ribosomal RNA suppresses streptomycin dependence and increases the frequency of translational errors. *Cell*, **66**, 141-148.
- Atmadja, J., Stiege, W., Zobawa, M., Greuer, B., Osswald, M. & Brimacombe, R. (1986). The tertiary folding of *Escherichia coli*: 16 S RNA, as studied by *in situ* intra-RNA cross-linking of 30 S ribosomal subunits with bis-(2-chloroethyl)-methylamine. *Nucl. Acids Res.* **14**, 659-673.
- Auffinger, P. & Westhof, E. (1999). Singly and bifurcated hydrogen-bonded base-pairs in tRNA anticodon hairpins and ribozymes. *J. Mol. Biol.* **292**, 467-483.
- Batey, R. T., Rambo, R. P., Lucast, L., Rha, B. & Doudna, J. A. (2000). Crystal structure of the ribonucleoprotein core of the signal recognition particle. *Science*, **287**, 1232-1239.
- Brosius, J., Ullrich, A., Raker, M. A., Gray, A., Dull, T. J., Gutell, R. R. & Noller, H. F. (1981). Construction and fine mapping of recombinant plasmids containing the *rrnB* ribosomal RNA operon of *E. coli*. *Plasmid*, **6**, 112-118.
- Brown, J. W., Nolan, J. M., Haas, E. S., Rubio, M. A., Major, F. & Pace, N. R. (1996). Comparative analysis of ribonuclease P RNA using gene sequences from natural microbial populations reveals tertiary structural elements. *Proc. Natl Acad. Sci. USA*, **93**, 3001-3006.
- Cate, J. H., Yusupov, M. M., Yusupova, G. Z., Earnest, T. N. & Noller, H. F. (1999). X-ray crystal structures of 70 S ribosome functional complexes. *Science*, **285**, 2095-2104.
- Chalfie, M., Tu, Y., Euskirchen, G., Ward, W. W. & Prasher, D. C. (1994). Green fluorescent protein as a marker for gene expression. *Science*, **263**, 802-805.
- Clarke, L. & Carbon, J. (1976). A colony bank containing synthetic Col El hybrid plasmids representative of the entire *E. coli* genome. *Cell*, **9**, 91-99.
- Clemons, W. M., Jr., May, J. L., Wimberly, B. T., McCutcheon, J. P., Capel, M. S. & Ramakrishnan, V. (1999). Structure of a bacterial 30S ribosomal subunit at 5.5 Å resolution. *Nature*, **400**, 833-840.
- Conn, G. L., Gutell, R. R. & Draper, D. E. (1998). A functional ribosomal RNA tertiary structure involves a base-triple interaction. *Biochemistry*, **37**, 11980-11988.
- Dong, H. & Kurland, C. G. (1995). Ribosome mutants with altered accuracy translate with reduced processivity. *J. Mol. Biol.* **248**, 551-561.
- Doring, T., Mitchell, P., Osswald, M., Bochkariov, D. & Brimacombe, R. (1994). The decoding region of 16 S RNA; a cross-linking study of the ribosomal A, P and E sites using tRNA derivatized at position 32 in the anticodon loop. *EMBO J.* **13**, 2677-2685.
- Dower, W. J., Miller, J. F. & Ragsdale, C. W. (1988). High efficiency transformation of *E. coli* by high voltage electroporation. *Nucl. Acids Res.* **16**, 6127-6145.
- Egebjerg, J. & Garrett, R. A. (1991). Binding sites of the antibiotics pactamycin and celesticetin on ribosomal RNAs. *Biochimie*, **73**, 1145-1149.
- Fountain, M. A., Serra, M. J., Krugh, T. R. & Turner, D. H. (1996). Structural features of a six-nucleotide RNA hairpin loop found in ribosomal RNA. *Biochemistry*, **35**, 6539-6548.
- Gautheret, D., Damberger, S. H. & Gutell, R. R. (1995). Identification of base-triples in RNA using comparative sequence analysis. *J. Mol. Biol.* **248**, 27-43.
- Gorini, L. (1971). Ribosomal discrimination of tRNAs. *Nature New Biol.* **234**, 261-264.
- Gutell, R. R. & Woese, C. R. (1990). Higher order structural elements in ribosomal RNAs: pseudo-knots and the use of noncanonical pairs. *Proc. Natl Acad. Sci. USA*, **87**, 663-667.
- Gutell, R. R., Larsen, N. & Woese, C. R. (1994). Lessons from an evolving rRNA: 16 S and 23 S rRNA structures from a comparative perspective. *Microbiol. Rev.* **58**, 10-26.
- Gutell, R. R., Cannone, J. J., Konings, D. & Gautheret, D. (2000). Predicting U-turns in ribosomal RNA with comparative sequence analysis. *J. Mol. Biol.* **300**, 791-803.
- Hanahan, D. (1983). Studies on transformation of *Escherichia coli* with plasmids. *J. Mol. Biol.* **166**, 557-580.
- Haselman, T., Camp, D. G. & Fox, G. E. (1989). Phylogenetic evidence for tertiary interactions in 16 S-like ribosomal RNA. *Nucl. Acids Res.* **17**, 2215-2221.
- Higuchi, R. (1989). Using PCR to engineer DNA. In *PCR Technology* (Erllich, H. A., ed.), pp. 61-70, Stockton Press, New York.
- Huang, S., Wang, Y. X. & Draper, D. E. (1996). Structure of a hexanucleotide RNA hairpin loop conserved in ribosomal RNAs. *J. Mol. Biol.* **258**, 308-321.
- Joseph, S., Weiser, B. & Noller, H. F. (1997). Mapping the inside of the ribosome with an RNA helical ruler. *Science*, **278**, 1093-1098.
- Jucker, F. M., Heus, H. A., Yip, P. F., Moors, E. H. & Pardi, A. (1996). A network of heterogeneous hydrogen bonds in GNRA tetraloops. *J. Mol. Biol.* **264**, 968-980.
- Larsen, N. (1992). Higher order interactions in 23 S rRNA. *Proc. Natl Acad. Sci. USA*, **89**, 5044-5048.
- Lee, K., Holland-Staley, C. A. & Cunningham, P. R. (1996). Genetic analysis of the Shine-Dalgarno interaction: selection of alternative functional mRNA-rRNA combinations. *RNA*, **2**, 1270-1285.
- Lee, K., Varma, S., SantaLucia, J., Jr & Cunningham, P. R. (1997). *In vivo* determination of RNA structure-function relationships: analysis of the 790 loop in ribosomal RNA. *J. Mol. Biol.* **269**, 732-743.
- Leontis, N. B. & Westhof, E. (1998a). The 5 S rRNA loop E: chemical probing and phylogenetic data versus crystal structure. *RNA*, **4**, 1134-1153.
- Leontis, N. B. & Westhof, E. (1998b). Conserved geometrical base-pairing patterns in RNA. *Quart. Rev. Biophys.* **31**, 399-455.
- Luria, S. E. & Burrous, J. W. (1957). Hybridization between *Escherichia coli* and *Shigella*. *J. Bacteriol.* **461-476**.
- Mankin, A. S. (1997). Pactamycin resistance mutations in functional sites of 16 S rRNA. *J. Mol. Biol.* **274**, 8-15.
- McCutcheon, J. P., Agrawal, R. K., Philips, S. M., Grassucci, R. A., Gerchman, S. E. & Clemons, W. M., Jr, *et al.* (1999). Location of translational initiation factor IF3 on the small ribosomal subunit. *Proc. Natl Acad. Sci. USA*, **96**, 4301-4306.
- Merryman, C., Moazed, D., McWhirter, J. & Noller, H. F. (1999). Nucleotides in 16 S rRNA protected by the association of 30 S and 50 S ribosomal subunits. *J. Mol. Biol.* **285**, 97-105.
- Michel, F. & Westhof, E. (1990). Modeling of the three-dimensional architecture of group I catalytic introns based on comparative sequence analysis. *J. Mol. Biol.* **216**, 585-610.

- Moazed, D. & Noller, H. F. (1986). Transfer RNA shields specific nucleotides in 16S ribosomal RNA from attack by chemical probes. *Cell*, **47**, 985-994.
- Moazed, D. & Noller, H. F. (1989). Intermediate states in the movement of transfer RNA in the ribosome. *Nature*, **342**, 142-148.
- Moazed, D. & Noller, H. F. (1990). Binding of tRNA to the ribosomal A and P sites protects two distinct sets of nucleotides in 16 S rRNA. *J. Mol. Biol.* **211**, 135-145.
- Morosyuk, S. V., Lee, K.-S., SantaLucia, J., Jr & Cunningham, P. R. (2000). Structure and function of the conserved 690 hairpin in *Escherichia coli*: 16 S ribosomal RNA. Analysis of the stem nucleotides. *J. Mol. Biol.* **300**, 113-126.
- Morosyuk, S. V., Cunningham, P. R. & SantaLucia, J., Jr. (2001). Structure and function of the conserved 690 hairpin in *Escherichia coli* 16 S ribosomal RNA: II. NMR solution structure. *J. Mol. Biol.* **307**, 197-211.
- Mueller, F. & Brimacombe, R. (1997). A new model for the three-dimensional folding of *Escherichia coli* 16 S ribosomal RNA. II. The RNA-protein interaction data. *J. Mol. Biol.* **271**, 545-565.
- Mueller, F., Stark, H., van Heel, M., Rinke-Appel, J. & Brimacombe, R. (1997). A new model for the three-dimensional folding of *Escherichia coli* 16 S ribosomal RNA. III. The topography of the functional centre. *J. Mol. Biol.* **271**, 566-587.
- Muralikrishna, P. & Wickstrom, E. (1989). *Escherichia coli* initiation factor 3 protein binding to 30 S ribosomal subunits alters the accessibility of nucleotides within the conserved central region of 16 S rRNA. *Biochemistry*, **28**, 7505-7510.
- Ninio, J. (1974). A semi-quantitative treatment of mis-sense and nonsense suppression in the *strA* and *ram* ribosomal mutants of *Escherichia coli*. Evaluation of some molecular parameters of translation *in vivo*. *J. Mol. Biol.* **84**, 297-313.
- O'Connor, M., Goring, H. U. & Dahlberg, A. E. (1992). A ribosomal ambiguity mutation in the 530 loop of *E. coli* 16 S rRNA. *Nucl. Acids Res.* **20**, 4221-4227.
- Oehler, R., Polacek, N., Steiner, G. & Barta, A. (1997). Interaction of tetracycline with RNA: photoincorporation into ribosomal RNA of *Escherichia coli*. *Nucl. Acids Res.* **25**, 1219-1224.
- Osswald, M., Doring, T. & Brimacombe, R. (1995). The ribosomal neighborhood of the central fold of tRNA: cross-links from position 47 of tRNA located at the A, P or E-site. *Nucl. Acids Res.* **23**, 4635-4641.
- Pettersson, I. & Kurland, C. G. (1980). Ribosomal protein L7/L12 is required for optimal translation. *Proc. Natl Acad. Sci. USA*, **77**, 4007-4010.
- Piepersberg, W., Nosedá, V. & Bock, A. (1979). Bacterial ribosomes with two ambiguity mutations: effects of translational fidelity on the response to aminoglycosides and on the rate of protein synthesis. *Mol. Gen. Genet.* **171**, 23-34.
- Pinard, R., Cote, M., Payant, C. & Brakier-Gingras, L. (1994). Positions 13 and 914 in *Escherichia coli* 16 S ribosomal RNA are involved in the control of translational accuracy. *Nucl. Acids Res.* **22**, 619-624.
- Pley, H. W., Flaherty, K. M. & McKay, D. B. (1994). Model for an RNA tertiary interaction from the structure of an intermolecular complex between a GAAA tetra-loop and an RNA helix. *Nature*, **372**, 111-113.
- Pon, C. L., Pawlik, R. T. & Gualerzi, C. (1982). The topographical localization of IF3 on *Escherichia coli* 30 S ribosomal subunits as a clue to its way of functioning. *FEBS Letters*, **137**, 163-167.
- Powers, T. & Noller, H. F. (1995). Hydroxyl radical footprinting of ribosomal proteins on 16 S rRNA. *RNA*, **1**, 194-209.
- Rinke-Appel, J., Junke, N., Osswald, M. & Brimacombe, R. (1995). The ribosomal environment of tRNA: crosslinks to rRNA from positions 8 and 20:1 in the central fold of tRNA located at the A, P, or E-site. *RNA*, **1**, 1018-1028.
- Ruusala, T., Andersson, D., Ehrenberg, M. & Kurland, C. G. (1984). Hyper-accurate ribosomes inhibit growth. *EMBO J.* **3**, 2575-2580.
- Schluenzen, F., Tocilj, A., Zarivach, R., Harms, J., Gluehmann, M. & Janell, D., *et al.* (2000). Structure of functionally activated small ribosomal subunit at 3.3 angstroms resolution. *Cell*, **102**, 615-623.
- Sprinzl, M., Steegborn, C., Hubel, F. & Steinberg, S. (1996). Compilation of tRNA sequences and sequences of tRNA genes. *Nucl. Acids Res.* **24**, 68-72.
- Stallings, S. C. & Moore, P. B. (1997). The structure of an essential splicing element: stem loop IIa from yeast U2 snRNA. *Structure*, **5**, 1173-1185.
- Stark, H., Orlova, E. V., Rinke-Appel, J., Junke, N., Mueller, F., Rodnina, M., Wintermeyer, W., Brimacombe, R. & van Heel, M. (1997). Arrangement of tRNAs in pre- and posttranslocational ribosomes revealed by electron cryomicroscopy. *Cell*, **88**, 19-28.
- Stern, S., Powers, T., Changchien, L. M. & Noller, H. F. (1988). Interaction of ribosomal proteins S5, S6, S11, S12, S18 and S21 with 16 S rRNA. *J. Mol. Biol.* **201**, 683-695.
- Stoffler-Meilicke, M. & Stoffler, G. (1987). The topography of ribosomal proteins on the surface of the 30 S subunit of *Escherichia coli*. *Biochimie*, **69**, 1049-1064.
- Su, L., Chen, L., Egli, M., Berger, J. M. & Rich, A. (1999). Minor groove RNA triplex in the crystal structure of a ribosomal frameshifting viral pseudoknot. *Nature Struct. Biol.* **6**, 285-292.
- Thompson, R. C. & Karim, A. M. (1982). The accuracy of protein biosynthesis is limited by its speed: high fidelity selection by ribosomes of aminoacyl-tRNA ternary complexes containing GTP[ $\gamma$ S]. *Proc. Natl Acad. Sci. USA*, **79**, 4922-4926.
- Van de Peer, Y., Robbrecht, E., de Hoog, S., Caers, A., De Rijk, P. & De Wachter, R. (1999). Database on the structure of small subunit ribosomal RNA. *Nucl. Acids Res.* **27**, 179-183.
- von Ahsen, U. & Noller, H. F. (1995). Identification of bases in 16 S rRNA essential for tRNA binding at the 30 S ribosomal P-site. *Science*, **267**, 234-237.
- Wimberly, B. T., Brodersen, D. E., Clemons, W. M., Jr, Morgan-Warren, R. J., Carter, A. P. & Vornrhein, C., *et al.* (2000). Structure of the 30 S ribosomal subunit. *Nature*, **407**, 327-339.
- Woodcock, J., Moazed, D., Cannon, M., Davies, J. & Noller, H. F. (1991). Interaction of antibiotics with A and P-site-specific bases in 16 S ribosomal RNA. *EMBO J.* **10**, 3099-3103.
- Zuker, M. (1989). On finding all suboptimal foldings of an RNA molecule. *Science*, **244**, 48-52.

Edited by I. Tinoco

(Received 4 August 2000; received in revised form 29 November 2000; accepted 25 December 2000)